J. Fluid Mech. (1967), *vol.* 29, *part* 1, *pp.* 113–135
Printed in Great Britain

The dynamics of turbulence near a wall according to a linear model

By GERALD SCHUBERT AND G. M. CORCOS
College of Engineering, University of California, Berkeley

(Received 6 July 1966)

The dynamics of turbulent velocity fluctuations in and somewhat outside the viscous sublayer are examined by linearizing the equations of motion around the known mean velocity profile. The rest of the boundary layer is assumed to drive the motion in the layer by means of a fluctuating pressure which is independent of distance from the wall. The equations, which are boundary-layer approximations to the Orr–Sommerfeld equations, are thus treated as a non-homogeneous system and solved by convergent power series. The solutions which exhibit the strong role of viscosity throughout the layer considered provide a model endowed with many of the known features of turbulence near a wall. In particular, the phase angle between streamwise and normal fluctuations is found to be in plausible agreement with experiments. An important role is ascribed by the solutions to the displacement of the mean velocity by the normal fluctuations. The impedance of the layer is found to be anisotropic in that it favours fluctuations with a much larger scale in the streamwise than in the spanwise direction. For such disturbances, the ratio of turbulent intensity to the intensity of the pressure fluctuations approximates the experimental ratio. According to the solutions it is primarily the spanwise component of the pressure gradient which is responsible for the intense level of turbulence very near the wall. The model apparently underestimates the amplitude ratio of normal to streamwise components of the velocity.

1. Introduction

Turbulent boundary layers are shear flows for which the presence of a solid boundary inhibits the turbulent motion in its immediate vicinity. The impervious wall and the no-slip condition insure that all components of the velocity vector vanish at the boundary and that the normal derivative of the normal component vanish there also. Nevertheless, it is an astonishing, though well-known fact that turbulence reaches a peak of intensity at a distance from the wall which does not exceed 2% of the boundary-layer thickness and which for high Reynolds numbers is far smaller than this value.

An interesting description has been given by Lighthill (1963) of the probable manner in which the vorticity of the mean flow is able to reach a very large and sharp peak at the wall and to combat the smoothing influence of diffusion. Lighthill appeals to the three-dimensional nature of the fluctuations and suggests that the wall correlates inflow normal to it with spanwise stretching which causes

the mean vorticity (directed spanwise) to be intensified while it is convected inward and weakened while it is transported outward. It is perhaps worth noting that almost any disturbance whose down-stream gradients are small next to its cross-stream gradients has this property if it satisfies continuity, whether it is dynamically possible or not. The burden of a dynamic model is to exhibit the phenomenon with sufficient quantitative accuracy and to account for the way in which a temporary increase in vorticity is contributed by the downward motion of the fluid particles or equivalently to produce large positive Reynolds stresses in the proximity of the wall.

Consider a two-dimensional incompressible turbulent boundary layer which is statistically stationary and adjacent to a plane, rigid and smooth wall. Decompose the velocity vector and the pressure into a time-independent and a time-dependent part

$$\mathbf{Q} = \langle \mathbf{Q}(\mathbf{r},t)\rangle + q(\mathbf{r},t) = \mathbf{U}(\mathbf{r}) + \mathbf{u}(\mathbf{r},t),$$
$$P(\mathbf{r},t) = \langle P\rangle + p(\mathbf{r},t),$$

where the brackets denote time averages. In cartesian co-ordinates, the equations of motion can be written

$$\frac{\partial u_i}{\partial t} + U_j \frac{\partial u_i}{\partial x_j} + u_j \frac{\partial U_i}{\partial x_j} + \frac{1}{\rho}\frac{\partial p}{\partial x_i} - \nu \frac{\partial^2 u_i}{\partial x_j^2} = \frac{1}{\rho}\frac{\partial \tau_{ij}}{\partial x_j}, \tag{1a}$$

$$\frac{\partial u_i}{\partial x_i} = 0, \tag{1b}$$

where $\tau_{ij} = \rho(\langle u_i u_j\rangle - u_i u_j)$, ν is the kinematic viscosity, ρ the constant density. Let x and z be the components of $\mathbf{r}$ in the downstream and spanwise directions and y the component normal to the wall. The corresponding mean and time-dependent velocity components are (U,u), $(0,w)$ and (V,v) respectively. It is known that throughout a layer extending from the wall to a distance y which includes roughly 15 % of the boundary-layer thickness (we will deal only with a region next to the wall which is far thinner) the law of the wall

$$U/u_\tau = f(yu_\tau/\nu)$$

applies. Here u_τ is the friction velocity $(\tau/\rho)^{\frac{1}{2}}$, where τ_w is the wall shear stress. An easily derived consequence of this empirical generalization is that

$$\frac{V}{U} = -\frac{y}{u_\tau}\frac{du_\tau}{dx}.$$

For a wide range of Reynolds numbers (Schlichting 1960) one finds that

$$\frac{d}{dx}\log u_\tau = \frac{1}{(\log U_\infty x/\nu - 0{\cdot}65)x},$$

where x is the apparent origin of the boundary layer. Thus for turbulent Reynolds numbers (say $U_\infty x/\nu > 5\times 10^5$)

$$\frac{d}{dx}\log u_\tau < \frac{1}{5x},$$

while, say for $yu_\tau/\nu < 100$, $y/x < 10^{-4}$, hence

$$V/U < 2\times 10^{-5},$$

while v/U is two or three orders of magnitude larger. We shall therefore neglect $V\,\partial u_i/\partial y$ in (1 *a*) and assume statistical homogeneity within planes parallel to the wall. The equations of motion in component form are thus

$$\left.\begin{aligned}
&\frac{\partial u}{\partial t}+U\frac{\partial u}{\partial x}+v\frac{\partial U}{\partial y}+\frac{1}{\rho}\frac{\partial p}{\partial x}-\nu\nabla^2 u=\frac{1}{\rho}\frac{\partial \tau_{xj}}{\partial x_j},\\
&\frac{\partial v}{\partial t}+U\frac{\partial v}{\partial x}\qquad\quad+\frac{1}{\rho}\frac{\partial p}{\partial y}-\nu\nabla^2 v=\frac{1}{\rho}\frac{\partial \tau_{yj}}{\partial x_j},\\
&\frac{\partial w}{\partial t}+U\frac{\partial w}{\partial x}\qquad\quad+\frac{1}{\rho}\frac{\partial p}{\partial z}-\nu\nabla^2 w=\frac{1}{\rho}\frac{\partial \tau_{zj}}{\partial x_j},\\
&\qquad\frac{\partial u}{\partial x}+\frac{\partial v}{\partial y}+\frac{\partial w}{\partial z}=0.
\end{aligned}\right\} \tag{2}$$

Since at the wall, $y=0$, $U=u=v=w=\partial v/\partial y=0$, as $y\to 0$ all quadratic terms are of higher order in y than the linear terms so that there must be a small region near the wall within which the asymptotic form of (2) is

$$\frac{\partial u_i}{\partial t}+\frac{1}{\rho}\frac{\partial p}{\partial x_i}-\nu\frac{\partial^2 u_i}{\partial x_j^2}=0. \tag{3}$$

Unfortunately the layer within which (3) is adequate turns out to be too thin for our purpose: (3) assumes that $\partial/\partial t \gg Q_j\,\partial/\partial x_j$, whereas $\partial/\partial t$ is of order U_0/λ, where U_0 is a characteristic velocity and λ a characteristic length for velocity gradients. Thus the assumption restricts us to a part of the flow wherein $Q_j \ll U_0$ and it is not suitable to investigate a region wherein, for instance, u reaches a maximum amplitude and U exceeds $\frac{1}{2}U_\infty$. A characteristic weakness of (3) is that it overestimates greatly the forces required to give rise to an apparent (local) acceleration. Thus the solutions of (3) given by Sternberg (1962) suggest a ratio of longitudinal pressure gradient to (downstream) velocity fluctuation amplitude which is excessively large. Another, related weakness of these solutions is that since the term $v\,\partial U/\partial y$, which represents the normal transport of mean momentum, is omitted, the basic mechanism which, one suspects, correlates normal and downstream velocity fluctuations of opposite signs and thus generates Reynolds stresses is absent so that the solutions fail to provide a mechanism by which a large mean vorticity gradient is maintained near the wall and by which the turbulence extracts energy from the mean flow. By allowing only vorticity diffusion to take place, (3) thus confines the role of the wall layer to that of a viscous damper. The models of Einstein & Li (1956), of Hanratty (1956) and of Sternberg (1962) were based on (3). The first two considered an intermittent layer whose growth in time by diffusion is interrupted by some kind of instability which brings the turbulent region into intimate contact with the wall after which the layer grows again, while Sternberg examined the behaviour of such a layer when it is continually excited by fluctuations at its outer edge. It is possible to consider a less radical type of linearization, that which consists in neglecting the right-hand side of (2) only. Such an approximation is also non-uniformly valid in that the relative importance of the neglected terms grows with the distance from the wall but as will be seen after the dynamics of the linear model have been clarified, it is likely

to fail only for values of yu_τ/ν which are substantially greater than those associated with the viscous sublayer.

It is apparent that while solutions of (2) are statistically stationary, solutions of the simpler homogeneous system obtained by eliminating the pressure and deleting the non-linear terms (the right-hand side of (2)) may not be. If U is assumed given, we may view these terms as forcing terms which trigger damped or growing oscillations of the linear system. A treatment along these lines has recently been summarized by Landahl (1965). All the eigenfunctions of the linear homogeneous system turn out to be stable and the space-time covariance of the pressure is analysed by assuming that the structure of the flow is governed by that of the least stable of the eigenfunctions, the non-linear terms affecting essentially only the amplitude of the solutions.

The approach used here resembles that of Landahl in that it omits the non-linear terms $\partial\tau_{ij}/\partial x_j$. It differs from his in that the formulation is not that of an eigenvalue problem solved throughout the boundary layer but that of a forced oscillation solved in a limited region near the wall. A similar treatment by Sternberg (1965) appeared after the present work was completed. It is discussed later on.

It is possible, as we shall see, to provide for the coupling with the outer flow without specifying outer boundary conditions which would prejudice the solution, i.e. which dictate either the location of the outer boundary (up to which linear approximations need be valid) or numerical values of the solution on that boundary. This is done by using the fluctuating pressure as the coupling variable.

2. The character of the pressure field near the wall

It has been shown (Corcos 1964) that the turbulent pressure fluctuations near the wall have two properties which will be used presently.

The first is that they are essentially independent of the normal co-ordinate y over a region $0 < y < y_0$ such that y_0 is substantially greater than the sublayer thickness. y_0 naturally depends on the spatial scale of the pressure disturbances. In a partial Fourier decomposition of the field in which the wave-number $\mathbf{k} = (k_x, k_z)$ corresponds to the position vector $\mathbf{r}_0 = (x, z)$, y_0 must be such that $ky_0 \ll 1$, the deviation from uniformity with y being equal to $(ky)^2$, where $k = |\mathbf{k}|$. For a laboratory boundary layer where the Reynolds number, based on displacement thickness, $Re\,\delta^* = 5 \times 10^4$ and where $U_\infty/u_\tau \cong 30$, the pressure energy spectrum, is found for $k\delta^* < 20$, it is possible to assume invariance of p with y with generally sufficient accuracy. For instance, since

$$\frac{y_0 u_\tau}{\nu} = \frac{ky_0}{k\delta^*}\frac{\delta^* U_\infty}{\nu}\frac{u_\tau}{U_\infty} = \frac{ky_0}{k\delta^*} \times 1{\cdot}66 \times 10^3,$$

the maximum error is 4 %, i.e.

$$ky \leqslant 0{\cdot}2 \quad \text{for} \quad k\delta^* = 1{\cdot}0 \quad \text{and} \quad y_0 u_\tau/\nu = 330$$
$$\text{and for} \quad k\delta^* = 10{\cdot}0 \quad \text{and} \quad y_0 u_\tau/\nu = 33.$$

At higher Reynolds numbers, the approximation is valid (at the same value of $k\delta^*$) for larger values of $y_0 u_\tau/\nu$.

The second property of the turbulent pressure near or at the wall is that it is related to velocity fluctuations which are not confined within the region we propose to study (say $yu_\tau/\nu < 50$). Evaluations of the covariance of the pressure at the wall in terms of the distribution of corresponding statistical functions of the velocity fluctuations have been made, using the integral relations corresponding to the Poisson equation for the pressure. In these evaluations, the integrand was either provided by a model of the velocity field (Lilley 1963) or by statistical measurements (Corcos 1964) and while the results did not agree in all respects, they suggested strongly that the sources of pressure spread over a region with thickness of order $10^3\nu/u_\tau$ and that the contribution of the inner tenth of that region is not considerable. In other words, at least in a coarse sense, one may view the turbulent pressure in the neighbourhood of the wall as the result of turbulence outside this thin layer and as driving the velocity fluctuations within it. This point of view suggests that we determine the velocity field in the wall layer in terms of a pressure field which is assumed given (and which may well be due to the non-linear dynamics outside the layer). We shall also assume the mean velocity profile as given and inquire later whether the computed fluctuating velocity field permits such a velocity profile to be maintained.

3. Equations

As a consequence of the approximate invariance of p with y in the thin wall layer we are entitled to use a boundary-layer form of the equations of motion. To the same approximation, viscous diffusion along the boundary may be omitted. The linear equations are then:

$$\left.\begin{aligned} \frac{\partial u}{\partial t}+U\frac{\partial u}{\partial x}+v\frac{dU}{dy} &= -\frac{1}{\rho}\frac{\partial p}{\partial x}+\nu\frac{\partial^2 u}{\partial y^2}, \\ \frac{\partial w}{\partial t}+U\frac{\partial w}{\partial x} &= -\frac{1}{\rho}\frac{\partial p}{\partial z}+\nu\frac{\partial^2 w}{\partial y^2}, \\ \frac{\partial u}{\partial x}+\frac{\partial v}{\partial y}+\frac{\partial w}{\partial z} &= 0. \end{aligned}\right\} \tag{4}$$

We then consider the fluctuating velocities and pressures to be a superposition of elementary disturbances whose amplitudes are functions of y, k_x, k_z and ω and whose phases are given by $\exp i(k_x x+k_z z+\omega t)$ where ω is the circular frequency. Define the phase velocity U_c of the disturbances as $U_c = -\omega/k_x$, and the complex amplitudes of the elementary disturbances by $\tilde{p}$, $\tilde{u}$, $\tilde{v}$, $\tilde{w}$. ($\tilde{p}$ is chosen as real.) The equations of motion become

$$\left.\begin{aligned} \frac{d^2\tilde{u}}{dy^2}-\frac{i}{\nu}(w+k_x U)\tilde{u}-\frac{1}{\nu}\frac{dU}{dy}\tilde{v} &= \frac{ik_x}{\mu}\tilde{p}, \\ \frac{d^2\tilde{w}}{dy^2}-\frac{i}{\nu}(w+k_x U)\tilde{w} &= \frac{ik_z}{\mu}\tilde{p}, \\ ik_x\tilde{u}+ik_z\tilde{w}+\frac{\partial\tilde{v}}{\partial y} &= 0, \end{aligned}\right\} \tag{5}$$

where $\tilde{p} = \tilde{p}_{\text{wall}}$ = a real constant. These equations (the boundary-layer approximations to the Orr–Sommerfeld equations) are to be treated here as non-homogeneous equations, the pressure fluctuation providing the driving force for the system. An equivalent set of equations which turns out to be somewhat more convenient to solve is obtained by eliminating the pressure:

$$\left.\begin{aligned} \frac{d^4\tilde{v}}{dy^4} - \frac{ik_x}{\nu}(U-U_c)\frac{d^2\tilde{v}}{dy^2} + \frac{ik_x}{\nu}\frac{d^2U}{dy^2}\tilde{v} &= 0, \\ \frac{d^3\tilde{w}}{dy^3} - \frac{ik_x}{\nu}(U-U_c)\frac{d\tilde{w}}{dy} - \frac{ik_x}{\nu}\frac{dU}{dy}\tilde{w} &= 0, \\ ik_x\tilde{u} + ik_z\tilde{w} + \frac{d\tilde{v}}{dy} &= 0. \end{aligned}\right\} \tag{6}$$

4. Boundary conditions

At the wall, $y = 0 : \tilde{w} = \tilde{v} = \partial\tilde{v}/\partial y = 0$. Also, (5) yields:

$$\frac{d^2\tilde{w}}{dy^2} = \frac{ik_z}{\mu}\tilde{p}; \quad \frac{d^3\tilde{w}}{dy^3} = \frac{k^2}{\mu}\tilde{p}.$$

We thus have three boundary conditions for the fourth-order v equation and two for the third-order w equation. The two additional conditions are provided as follows: it seems natural to require that the effect of viscosity does not dominate the solutions as $y \to \infty$. It can be anticipated that $\tilde{v}$ and $\tilde{w}$ may be obtained from the superposition of linearly independent solutions of (6) (four for $\tilde{v}$, three for $\tilde{w}$). One solution for each component increases asymptotically with y as an exponential involving the viscosity coefficient and whose real part is positive. Such solutions should be rejected but the manner in which it should be done is perhaps best seen after the role of the critical point has been discussed.

5. The critical point

It is known from stability theory that viscosity plays a predominant role in determining the solutions of (6) in two regions: near the wall, and in the neighbourhood of the so-called critical point, the value y_c of y, if any, for which $U = -\omega/k_x$. These regions are broader than they are usually in laminar stability theory, so that inviscid approximations are not justified anywhere in the region of interest and will not be used. One might conceive the proper solution of (6) as that which satisfies the wall-boundary conditions and for which, as $y > y_c$, the contribution from the exponentially increasing viscous solution would be excluded. If we considered the linear approximation (6) to be as valid far from the wall as it is near the wall, this would indeed be the only possible point of view. But it is known that a typical turbulent component of a given frequency travels downstream at a wave velocity such that $y_c u_\tau/\nu > 100$, so that the outer boundary condition would have to be applied in a region where (as is shown later) nonlinear terms are almost sure to render (6) quite inaccurate. It thus seems preferable to forego a solution which extends beyond the critical point and merely select the combination of solutions for which the effect of viscosity decreases

fastest as y increases. This selection is dictated by the belief, generally held, that the effect of viscosity upon the fluctuating velocity field is small for $yu_\tau/\nu > 40$.

In order to solve (6) analytically it is expedient to approximate the velocity profile in the inner region (say $yu_\tau/\nu \leqslant 50$) by the simple form

$$U/u_\tau = \beta\left[1-\exp\left(-\frac{yu_\tau}{\beta\nu}\right)\right]. \tag{7}$$

It is compared in table 1 with the law of the wall, according to a careful study of experimental results by Coles (1953). The value of β chosen is 16·0.

yu_τ/ν	$U/u_\tau = \beta\left[1-\exp\left(-\frac{yu_\tau}{\beta\nu}\right)\right]$	Law of wall
0	0	0
2	1·88	1·96
4	3·54	3·80
6	5·00	5·45
8	6·30	6·87
10	7·44	8·05
20	11·42	11·49
40	14·69	14·22
60	15·62	15·33
80	15·89	16·04
100	15·97	16·60

TABLE 1

6. The solutions for the exponential mean velocity profile

If the mean velocity is given by (7), the transformation

$$Y = \exp-(yu_\tau/\beta\nu)$$

casts the interval $0 \leqslant y < \infty$ into the interval $1 \geqslant Y > 0$ and it becomes a simple matter to examine the asymptotic behaviour of the linearly independent solutions for large y. Define

$$\gamma = 1 - U_c/\beta u_\tau; \quad \alpha = k_x \nu \beta^3/u_\tau.$$

The four independent solutions of $\tilde{v}$ are found to be a polynomial and three absolutely convergent power series, i.e.:

(*a*) $\gamma\left(1+\frac{i}{\alpha\gamma}\right) - Y,$

(*b*) $Y\ln Y - \gamma\left\{1+\frac{i}{\alpha\gamma}\right\}(1+\ln Y) + \sum_{n=1}^{\infty} a_n Y^n,$

where
$$a_1 = \frac{\alpha\gamma+3i}{\alpha\gamma+i}; \quad a_2 = \frac{1}{2\gamma}\left\{\frac{\gamma}{\alpha\gamma+4i}\right\},$$

$$a_n = a_{n+1}\left(\frac{n-2}{n}\right)\frac{1}{\gamma}\left\{\frac{\alpha\gamma}{\alpha\gamma+in^2}\right\}, \quad \text{for} \quad n \geqslant 3,$$

(*c*) $\sum_{n=0}^{\infty} b_n Y^{\eta+n},$

where $\eta = (i\alpha\gamma)^{\frac{1}{2}}$. η is chosen to have a positive real part and

$$b_0 = 1, \quad b_n = b_{n-1} i\alpha \frac{2-(\eta+n)}{(\eta+n)[(\eta+n)^2 - i\alpha\gamma]},$$

(*d*) the series obtained from (*c*) above but with η replaced everywhere by $-\eta$.

A similar approach leads to three independent solutions for $\tilde{w}$, i.e.:

(*a*) $\sum_{n=0}^{\infty} c_n Y^n$,

where $c_0 = 1$ and for $n \geqslant 1$, $c_n = c_{n-1} \frac{\gamma}{1 + in^2/\alpha\gamma}$,

(*b*) $\sum_{n=0}^{\infty} d_n Y^{\eta+n}$,

where $d_0 = 1$ and for $n \geqslant 1$, $d_n = d_{n-1} \frac{-i\alpha}{(\eta+n)^2 - i\alpha\gamma}$,

(*c*) the series obtained from (*b*) above by replacing η everywhere by $-\eta$. Both solutions (*d*) for v and (*c*) for w diverge exponentially as $y \to \infty$ and they will be discarded in accordance with our outer boundary conditions.

The foregoing solutions were derived under the restriction $U_c/u_\tau \neq \beta$. The solutions for $U_c/u_\tau = \beta$ are of little interest since one value of β has no more physical significance than a neighbouring one.

7. The inviscid limit

The inviscid version of equations (5) is

$$\left.\begin{aligned} \tilde{w} &= -\frac{k_z}{k_x}\frac{p}{\rho}\frac{1}{U-U_c}, \\ -ik_x(U-U_c)\tilde{u} &= \frac{dU}{dy}\tilde{v} + \frac{ik_x}{\rho}\tilde{p}, \\ ik_x\tilde{u} + ik_z\tilde{w} + \frac{d\tilde{v}}{dy} &= 0. \end{aligned}\right\} \tag{8}$$

It is of interest to compare the solutions of these equations with the solutions we have obtained, in order to establish in what sense the effect of viscosity becomes small as y grows large. The former can be written explicitly and in finite form for exponential mean velocity profile, but for purposes of comparison it is preferable to work with the two linearly independent solutions of the inviscid equation for $\tilde{v}$,

$$(U-U_c)\frac{d^2\tilde{v}}{dy^2} - \tilde{v}\frac{d^2U}{dy^2} = 0.$$

Those are

(a') $\gamma - Y$, and

(b') $-\gamma + \ln Y(Y-\beta) + (\beta - Y)\log(\pm\gamma \mp Y)$.

The first two solutions of the complete equations for $\tilde{v}$ are those related to these

inviscid solutions. They are found to tend to the latter as $\alpha\gamma \to \infty$† if $Y < |\gamma|$. The second condition is required for the expansion

$$\log\left(1-\frac{Y}{\gamma}\right) = -\sum_{n=1}^{\infty}\frac{Y^n}{n\gamma^n}$$

if we take the argument of the logarithm to be positive. Solution (a) for $\tilde{v}$ tends to (a') above for all values of y as $|\alpha\gamma|$ becomes large. However solution (b) converges for all values of y because the parameter $\alpha\gamma$ is finite. Thus in order for (b) to approach its inviscid counterpart (b'), the convergence must be essentially complete for values of n smaller than that for which $(1+in^2/\alpha\gamma)$ is significantly different from unity. This requires that $|\alpha\gamma|$ be large and that y be large enough so that $Y < |\gamma|$. The latter requirement is equivalent to

$$U > U_c, \quad \left(\frac{U_c}{\beta u_\tau} < 1\right);$$

$$\frac{U}{\beta u_\tau} > 2-\frac{U_c}{\beta u_\tau}, \quad \left(\frac{U_c}{\beta u_\tau} > 1\right);$$

and implies that no matter how large $|\alpha\gamma|$, (b) does not tend to (b') near the wall. Finally, the third (viscous) solution decays as yu_τ/ν increases, as indicated by the factor

$$\exp-\left[-\frac{yu_\tau}{\nu}\frac{1+i}{\sqrt{2}}|\alpha\gamma|^{\frac{1}{2}}\right].$$

In this connexion, it should be noted that the thickness of the viscous inner layer is large, primarily because the coefficient of the second-order term for $\tilde{v}$ (or of the first-order term for $\tilde{w}$), rapidly decreases as y increases. This is a consequence of the very abrupt rise in the mean velocity near the wall. For instance, assume a laboratory layer for which $\delta^* u_\tau/\nu = 1600$ and choose $\beta = 16$, $U_c = 20u_\tau$ and $k_x\delta^* = 1{\cdot}0$. For this case, the exponential factor for the viscous solution of (3) (equations which omit mean convection) is $yu_\tau/5{\cdot}7\nu$, while the exponential factor for the profile chosen above is $yu_\tau/28\nu$.

It is thus seen that the solution of equations (6) tends to the solution of the inviscid equations under well-defined conditions, which have just been given, but that for the range of wave numbers which is relevant to turbulence, this tendency is weak enough so that for all but the shortest wavelengths, the effect of viscosity permeates the layer $yu_\tau/\nu < 50$.

8. Calculation of the solutions

Numerical solutions of (6) have been obtained by combining linearly the first three fundamental solutions for $\tilde{v}$ so that their sum satisfies the boundary conditions at the wall. The same is done for the first two fundamental solutions of $\tilde{w}$. The series are summed with the aid of an I.B.M. 7090 computer. They are found

† At first sight it may seem paradoxical that $\alpha\gamma \to \infty$ is an inviscid limit since it can be obtained by letting $\nu \to \infty$. But the reader should keep in mind that for the mean flow a viscous length is proportional to ν while for a disturbance it is only proportional to $\nu^{\frac{1}{2}}$ according to the linearized equations. The limit above is then a proper inviscid limit for the disturbance in law of the wall co-ordinates.

to converge rapidly enough and the accuracy of the machine is not taxed unless the parameter $\alpha\gamma$ is excessively large. The program was able to generate thirty terms for each series, but only rarely were more than ten or fifteen terms required. The computation yields for chosen values of k_x, k_z and ω, the complex functions $\tilde{u}$, $\tilde{v}$, $\tilde{w}$, $\tilde{u}-\tilde{w}$ and the Reynolds stresses $-\{\mathscr{R}(\tilde{u})\,\mathscr{R}(\tilde{v})+\mathscr{I}(\tilde{u})\,\mathscr{I}(\tilde{v})\}$ where $\mathscr{R}$ and $\mathscr{I}$ are the real and imaginary parts respectively.

9. The parameter k_z

Given the solutions for a chosen value of k_x and ω, and a non-zero value of k_z, the solutions for any other value of k_z are immediately accessible.

Let two such cases be denoted by the subscripts 1 and 2. The homogeneous equations for $\tilde{v}$ and $\tilde{w}$, equations (6), are independent of k_z, so that the fundamental solutions for these velocity components must be the same. The value of k_z only affects the boundary conditions. The inhomogeneous boundary condition on $\tilde{v}$ requires that

$$\frac{\tilde{v}_2}{\tilde{v}_1}=\frac{k_x^2+(k_z)_2^2}{k_x^2+(k_z)_1^2}, \tag{9}$$

and that for $\tilde{w}$ leads to

$$\tilde{w}_2/\tilde{w}_1=(k_z)_2/(k_z)_1. \tag{10}$$

Finally, from the continuity equation, we find that

$$\tilde{u}_2=\tilde{u}_1\frac{k_x^2+(k_z)_2^2}{k_x^2+(k_z)_1^2}+\tilde{w}_1\frac{k_x}{(k_z)_1}\frac{(k_z)_1^2-(k_z)_2^2}{(k_x)^2+(k_z)_1^2}. \tag{11}$$

From relations (9) and (10) one notes that by changing the value of k_z (k_x and w remaining fixed) one merely multiplies solutions for $\tilde{v}$ and $\tilde{w}$ by a constant real factor, so that the phase of $\tilde{v}$ and $\tilde{w}$ with respect to $\tilde{p}$ at any y is independent of k_z. It is also apparent that the amplitude of $\tilde{v}$ and $\tilde{w}$ increases with k_z.

The numerical solutions were all obtained for $k_z=k_x$, for the reason that the difference between the functions $\tilde{u}$ and $\tilde{w}$ is for this case entirely due to the term $\tilde{v}\,dU/dy$ in (6), i.e. to the normal transport of mean momentum by the fluctuating velocity component $\tilde{v}$. If we now choose $(k_z)_1=k_x$ and define $(k_z)_2=k_z$, we find that when $k_z/k_x\ll 1$,

$$\tilde{v}_2/\tilde{v}_1=\tfrac{1}{2}\{1+(k_z/k_x)^2\}\sim\tfrac{1}{2}, \tag{12a}$$

$$\tilde{w}_2/\tilde{w}_1=k_z/k_x\to 0, \tag{12b}$$

$$\tilde{u}_2\sim\tfrac{1}{2}(\tilde{u}_1+\tilde{w}_1), \tag{12c}$$

while when $k_c/k_x\gg 1$,

$$\tilde{v}_2/\tilde{v}_1\sim\tfrac{1}{2}(k_z/k_x)^2, \tag{13a}$$

$$\tilde{u}_2=\tfrac{1}{2}[(\tilde{u}_1+w_1)+(k_z/k_x)^2(\tilde{u}_1-\tilde{w}_1)]\sim\tfrac{1}{2}(k_z/k_x)^2(\tilde{u}_1-\tilde{w}_1), \tag{13b}$$

$$\tilde{w}_2/\tilde{w}_1=k_z/k_x. \tag{13c}$$

Thus $\tilde{w}/\tilde{u}$ disappears in both limits $k_z/k_x\to 0$ and $k_z/k_x\to\infty$. Note also that for wave-number vectors which have a predominant component in the spanwise direction (disturbances which are highly elongated in the downstream direction), the downstream component is proportional to the difference between $\tilde{u}_1$ and $\tilde{w}_1$ (components for $k_z=k_x$). This result has both a simple physical explanation and important consequences which will be discussed later.

10. The pressure field

The solutions which have been computed are functions of the normal distance $y^* = yu_\tau/\nu$ for arbitrary choices of the frequency ω and of the wave-number $\mathbf{k} = (k_x, k_z)$. These functions (e.g. $\tilde{u}, \hat{v}, \hat{w}$) are generalized Fourier transforms of the random velocity components u, v, w, non-dimensionalized by the driving pressure amplitude $\tilde{p}$ (the Fourier transform of the fluctuating pressure), by the density and by the friction velocity u_τ. Their real part denotes that part which is in phase with the pressure, their imaginary part, that part which is $\frac{1}{2}\pi$ radians out of phase with it.

If the three-dimensional spectrum $\Pi(k_x, k_z, \omega)$ of the wall pressure were sufficiently well known from experiments, it would be possible to construct from the elementary solutions, the three-dimensional spectrum of the velocity components and, by integration, the mean square of these components. For instance, since

$$\begin{matrix}\Pi(\mathbf{k},\omega)\\ E_u(\mathbf{k},\omega)\end{matrix}\delta(\mathbf{k}-\mathbf{k}',\omega-\omega') = \left\langle\begin{matrix}\tilde{p}(\mathbf{k},\omega)\,\tilde{p}^*(\mathbf{k}',\omega')\\ \tilde{u}(\mathbf{k},\omega)\,\tilde{u}(\mathbf{k}',\omega')\end{matrix}\right\rangle,$$

$$\rho^2 u_\tau^2 E_u/\Pi(\mathbf{k},\omega) = \tilde{u}(\mathbf{k},\omega)\,\hat{u}^*(\mathbf{k},\omega),$$

where a star denotes a complex conjugate and the brackets an ensemble average, and where $\hat{u} = \rho\tilde{u}u_\tau/\tilde{p}$.

We summarize here some of the pertinent results of observations concerning the turbulent pressure.

For two-dimensional turbulent boundary layers in the absence of mean pressure gradients, numerous experiments indicate (see, for example, Corcos 1964) that the root mean square of the pressure intensity at the wall is related to the wall shear stress by

$$\sqrt{\langle p^2\rangle} = (3{\cdot}0 \pm 0{\cdot}5)\tau_w.$$

From the space covariances of the wall pressure (Bull, Wilby & Blackman 1963), one may construct approximately the two-dimensional (k_x, k_z) spectrum $G(k_x, k_z)$ of the pressure. It is shown in figure 1 and suggests that the spectral power density of the driving force for the velocity fluctuations is almost symmetrically distributed with respect to $\theta = \frac{1}{4}\pi$. Somewhat more energy is found near $\theta = 0$ and $\theta = \frac{1}{2}\pi$ than around $\theta = \frac{1}{4}\pi$. However, the data are too coarse to provide unambiguous information about the important asymptotic behaviour of the spectrum,

$$\lim_{\substack{k_z \text{ fixed}\\ k_x \to 0}} G(k_x, k_z).$$

Experimentally plausible alternate contours are shown as dotted lines.

From the reported values of the space-time covariance of the wall pressure and of its cross-spectral density (Bull *et al.* 1963; Willmarth & Wooldridge 1962; Priestly 1965) it is possible to construct coarse approximations to the three-dimensional spectrum Π itself. It is perhaps sufficient to indicate the main feature of this three-dimensional spectrum: $\Pi(k_x, k_z, \omega)$ reveals a statistically pre-

ferred wave speed U_0 which is a gently decreasing function of frequency and which is usually given in terms of the free stream velocity (roughly, $0{\cdot}60 < U_0/U_\infty < 0{\cdot}80$). In other words, the integration of $\Pi(k_x, k_z, \omega)$ over ω contributes little to G except within a small range of $(-\omega/k_x)$ centred around U_0.

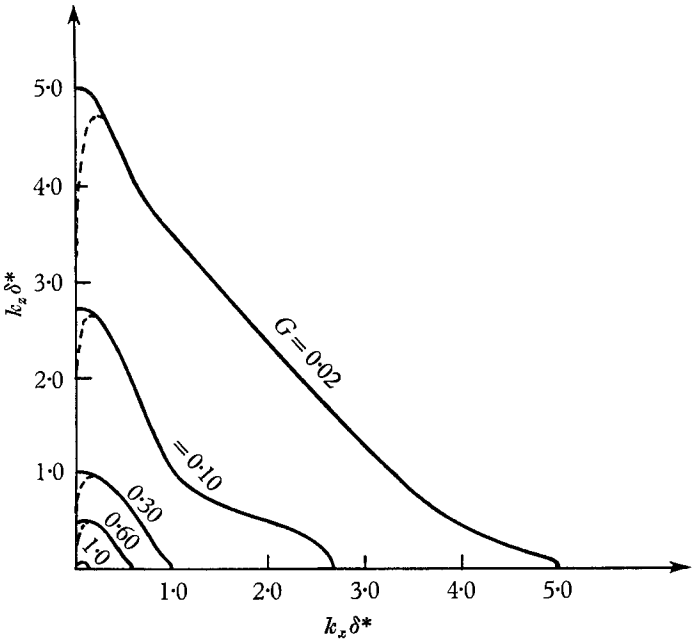

FIGURE 1. The wall pressure spectrum, $G(k_x, k_z)$ (units of density arbitrary).

11. The fluctuating velocity field

For purposes of comparison with the computed solutions, some experimentally recorded features of the velocity fluctuations are shown below. Figure 2 is a replot of data by Klebanoff (1954) in which the root mean square of the velocity fluctuations, non-dimensionalized by the friction velocity and the (presumed) turbulent pressure intensity are given as a function of viscous distance from the wall. u' is seen to peak at $y^* = 25$, while w' reaches a maximum further ($y^* \cong 60$) and v' does not reach a maximum until $y^* \cong 600$. Table 2 gives an idea of the square root spectral density ratios as a function of longitudinal wave-number k_x. It was obtained from available measurements of the one-dimensional spectrum of pressure at the wall (Bull *et al.* 1963) and from Klebanoff's measurements of one-dimensional spectra of velocities at $y^* = 150$ (which is unfortunately the closest point at which measurements of v' and w' have been reported to date for a boundary layer). Because the shape of the velocity spectra is likely to vary significantly as the wall is approached, and because there is only fair agreement between experimenters about fluctuation levels and spectra these measurements should be taken as indicating order of magnitude only, a factor of two error being possible, a factor of ten error, unlikely (table 2).

Finally, both Klebanoff's measurements of root mean square gradients of velocity fluctuation ($y^* = 50$) and Grant's (1958) measurements of longitudinal and spanwise covariances ($y^* = 30$, $y^* = 60$) indicate that the longitudinal scale of the downstream component u is large next to the spanwise scale, which implies that in a Fourier decomposition of the velocity field, contributions to the two-dimensional k_x, k_z spectrum occur primarily from high values of the ratio k_z/k_x. The same is true of v while for w the scales are more nearly equal.

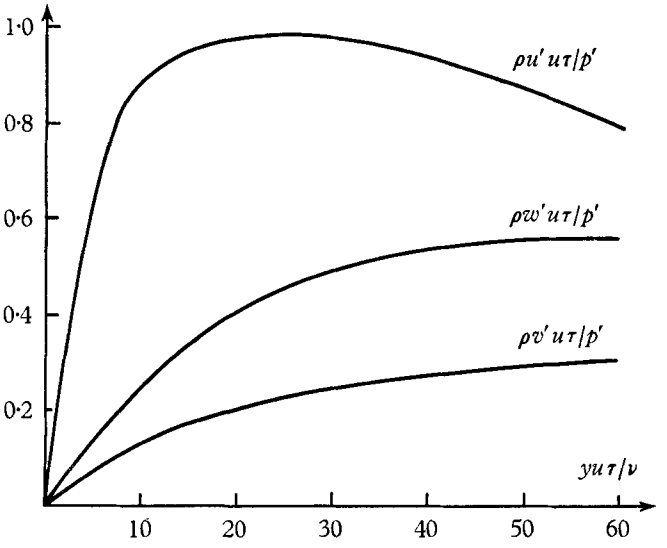

FIGURE 2. The distribution of the root-mean square of velocity fluctuations near the wall (from Klebanoff 1954).

k_x	f_u	f_v	f_w	$f\langle uv\rangle$
0·1	1·02	0·170		0·61
0·4	0·68	0·147		0·65
1·0	0·75	0·180	Average = 0·490	0·45
4·0	1·05	0·240		0·40
10·0	1·44	0·472		0·28

TABLE 2. f_u, f_v and f_w are the square root of the one-dimensional spectra of u', v', w' normalized by the square root of the one-dimensional wall pressure spectrum and the factor ρu_τ. $f_{uv}(k_x)$ is the one-dimensional spectrum of the Reynolds stresses, non-dimensionalized by the square root of the product of the spectra of u' and v'. The functions are estimated at $y^* = 30$.

12. Solutions for $k_x = k_z$

Solutions have been obtained for $k_x\delta^* = 0{\cdot}1$, 1·0, 4·0 and 10·0 with values of ω such that the wave speed is equal to the local mean velocity at values of y_c^* ranging from 100 to 1000, which correspond to $16 \leqslant U_c/u_\tau \leqslant 23$. For a boundary layer with Reynolds number $R_{\delta^*} = 50{,}000$, this corresponds to

$$0{\cdot}52 \leqslant U_c/U_\infty \leqslant 0{\cdot}74$$

and for a boundary layer such as that of Klebanoff with $R_{\delta^*} \cong 10{,}000$ to

$$0{\cdot}6 \leqslant U_c/U_\infty \leqslant 0{\cdot}86.$$

In all cases, even when the wave speed is larger than the asymptotic value βu_τ of the inner representation for the veolocity profile, the values of y_c^* given above are to be interpreted as those for which the law of the wall yields a mean velocity equal to the chosen phase velocity.

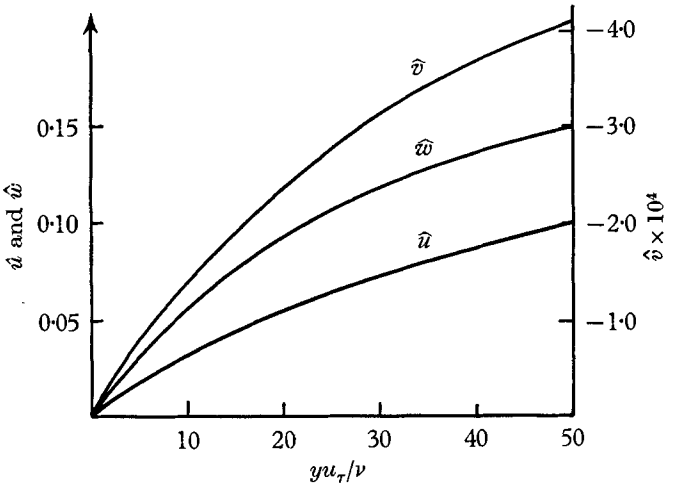

FIGURE 3. The real parts of $\hat{u}$, $\hat{v}$ and $\hat{w}$ for $k_x\delta^* = k_z\delta^* = 1{\cdot}0$ and $y_c^* = 800$.

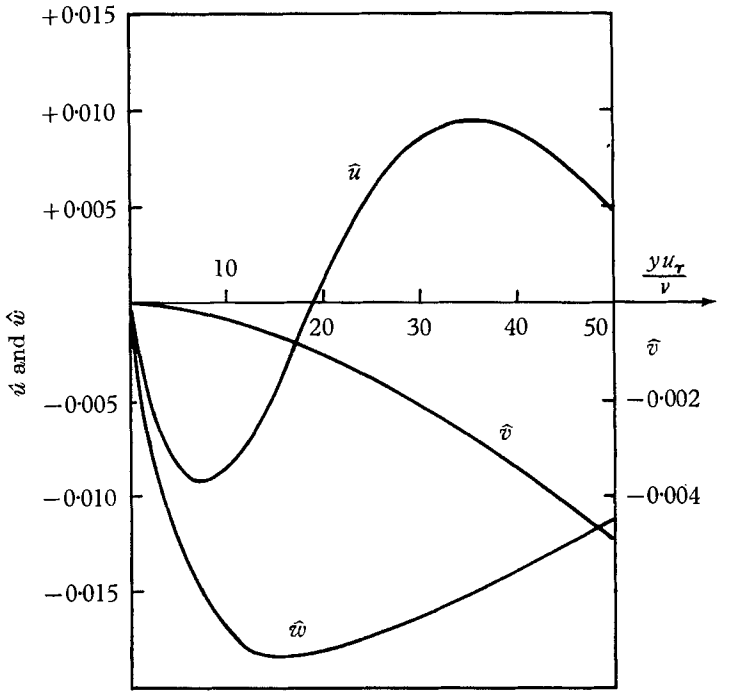

FIGURE 4. The imaginary parts of $\hat{u}$, $\hat{v}$ and $\hat{w}$ for $k_x\delta^* = k_z\delta^* = 1{\cdot}0$ and $y_c^* = 800$.

Figures 3 and 4 show the real and imaginary parts of the three velocity components for the case $k_x\delta^* = 1{\cdot}0$; $y_c^* = 800$. The real parts of $\hat{u}$ and $\hat{w}$ are positive and much larger than their imaginary parts. $\mathscr{R}(\hat{w})$ is larger than $\mathscr{R}(\hat{u})$ and both functions are monotonic within the interval $0 < y^* < 50$. $\mathscr{I}(\hat{v}) \gg \mathscr{R}(\hat{v})$ and $\hat{v}$ is extremely small. Since $\tilde{u}$ is almost in phase with $\tilde{p}$ while $\tilde{v}$ is about $-\frac{1}{2}\pi$ out of phase with $\tilde{p}$, the Reynolds stress coefficient, $C_R = -\langle\hat{u}\hat{v}\rangle/|\hat{u}||\hat{v}|$ is small. These features of the solution are typical of all the solutions investigated for which $y_c^* > 50$ and $0{\cdot}1 \leqslant k_x\delta^* \leqslant 4$, although there are minor variations in the phases of $\hat{u}$ and $\hat{w}$ ($\tilde{u}$ may lead or lag $\tilde{p}$ by fifteen or twenty degrees). There is no tendency for the amplitude of the solutions to reach a maximum and no definable region which one might identify as a viscous sublayer. Table 3 lists the values of the solutions

$k_x\delta^*$	y_c^*	$\mathscr{R}(\hat{u})$	$\mathscr{I}(\hat{u})$	$\mathscr{R}(\hat{v})$	$\mathscr{I}(\hat{v})$	$\mathscr{R}(\hat{w})$	$\mathscr{I}(\hat{w})$
0·1	500	+0·073	−0·029	−0·00006	−0·00014	+0·076	−0·043
0·1	800	+0·064	−0·024	−0·00006	−0·00013	+0·066	−0·037
0·1	1000	+0·060	−0·021	−0·00007	−0·00012	+0·063	−0·035
1·0	100	+0·270	+0·050	+0·0010	−0·0040	+0·565	−0·090
1·0	200	+0·095	+0·016	−0·00012	−0·0030	+0·23	−0·030
1·0	500	+0·079	+0·012	−0·00032	−0·0023	+0·140	−0·0195
1·0	800	+0·071	+0·0087	−0·00032	−0·0021	+0·121	−0·0160
1·0	1000	+0·071	+0·0076	−0·00032	−0·0021	+0·113	−0·015
4·0	200	+0·061	+0·023	0	−0·0050	+0·215	−0·0015
4·0	500	+0·059	+0·011	−0·00032	−0·010	+0·142	−0·0025
4·0	800	+0·057	+0·009	−0·00036	−0·0125	+0·122	−0·0020
10·0	1000	+0·053	+0·0025	−0·00044	−0·0210	+0·113	−0·0010

TABLE 3. The values of $\hat{u}$, $\hat{v}$ and $\hat{w}$ for $k_z = k_x$, $y^* = 30$.

at $y^* = 30$. A comparison of these values with those in table 2 (averaged over k_x and ω) and with those of figure 2 (averaged over k_x, k_z, ω) indicates that while the values of $\hat{w}$ given by the solutions are only somewhat too small, the values of $\tilde{u}$ and $\tilde{v}$ are much too small to be representative of a typical velocity component. The discrepancy is a factor of at least 10 for $\tilde{u}$ and at least 20 for $\tilde{v}$. It is readily seen from (13) that neither the general shape of $\hat{u}$ and $\hat{v}$ nor their order of magnitude are affected if $k_z \ll k_x$ while of course $\hat{w}$ decreases linearly with k_z.

The solutions for $\hat{u}$ and $\hat{w}$ with $k_x\delta^* = k_z\delta^* = 10$, $y_c^* = 1000$, are shown in figure 5. For these values of the parameters, the viscous length is small so that the effect of viscosity is confined to a region relatively near the wall. Only in such cases do the solutions exhibit a viscous sublayer. Note that beyond this sublayer $\hat{u}$ and $\hat{w}$ are almost purely real. As a result the Reynolds stresses are extremely small.

Thus solutions of the linearized equations for $\tan\theta = k_z/k_x \leqslant 1$ cannot contribute measurably to the Reynolds stresses which are required to maintain the assumed mean velocity profile or to the distribution of u' and v' which is observed. On the other hand, as we have seen, experimental observations have established that near the wall, the spatial structure of u' and v' is very elongated in the streamwise direction so that the spectra should receive most of their energy from waves

such that $\tan\theta \gg 1$. It is thus necessary to determine what happens to the solutions as k_z/k_x becomes large. According to (13 *b*)

$$\hat{u} \simeq \frac{1}{2}\left(\frac{k_z}{k_x}\right)^2 (\hat{u}_1 - \hat{w}_1), \quad k_z/k_x \gg 1, \quad \begin{Bmatrix} u_1 \\ w_1 \end{Bmatrix} \equiv \begin{Bmatrix} u \\ w \end{Bmatrix}_{k_z=k_x}.$$

Figures 6–8 are plots of $(\hat{u}_1 - \hat{w}_1)$ in these groups. Figure 6 shows moderate and high wave-numbers and moderate wave velocities; figure 7 small wave velocities; figure 8 small wave-numbers. The graphs reveal that the magnitude of $\hat{u}$ for large

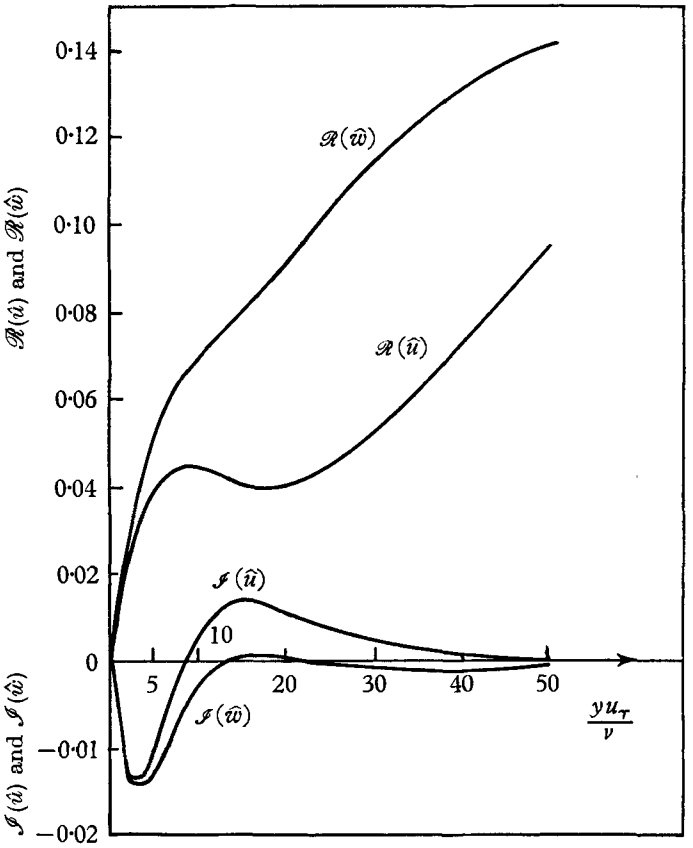

FIGURE 5. The real and imaginary parts of $\hat{u}$ and $\hat{w}$ for $k_x\delta^* = k_z\delta^* = 10$ and $y_c^* = 1000$.

values of θ rises to a peak which is found for $25 < y^* < 50$. The peak is closer to the wall for large $k_x\delta^*$ and large y_c^* and recedes with increasing values of both parameters, but considering that the wave-number range shown is a 100 to 1, the location of the peak is dispersed relatively little by these parameters. The fact that $\mathscr{I}(\hat{u}_1 - \hat{w}_1)$ achieves its peak value for smaller values of y^* than $\mathscr{R}(\hat{u}_1 - \hat{w}_1)$ is also significant; since $\hat{v}$ is in general almost purely imaginary, the Reynolds stresses are contributed primarily by the product $\mathscr{I}(\hat{v})$ and $\mathscr{I}(\hat{u})$. In general $\mathscr{R}(\hat{u}_1 - \hat{w}_1)$ is negative which indicates that the phase angle of $\tilde{u}$ with respect to $\tilde{p}$ changes from a small value for $\theta < \frac{1}{4}\pi$ to a value exceeding $\frac{1}{2}\pi$ for $\theta \to \frac{1}{2}\pi$. The

value of θ for which $\hat{u}$ is purely imaginary generally increases with y^* for given values of k_x and ω and in some cases the real part of $\hat{u}$ does not change sign for sufficiently large values of y^*.

We have used (9), (10) and (11) to compute $\hat{u}$, $\tilde{v}$, $\hat{w}$ and the Reynolds stress coefficient C_R for several values of $k_x\delta^*$ after choosing a value of θ for each case

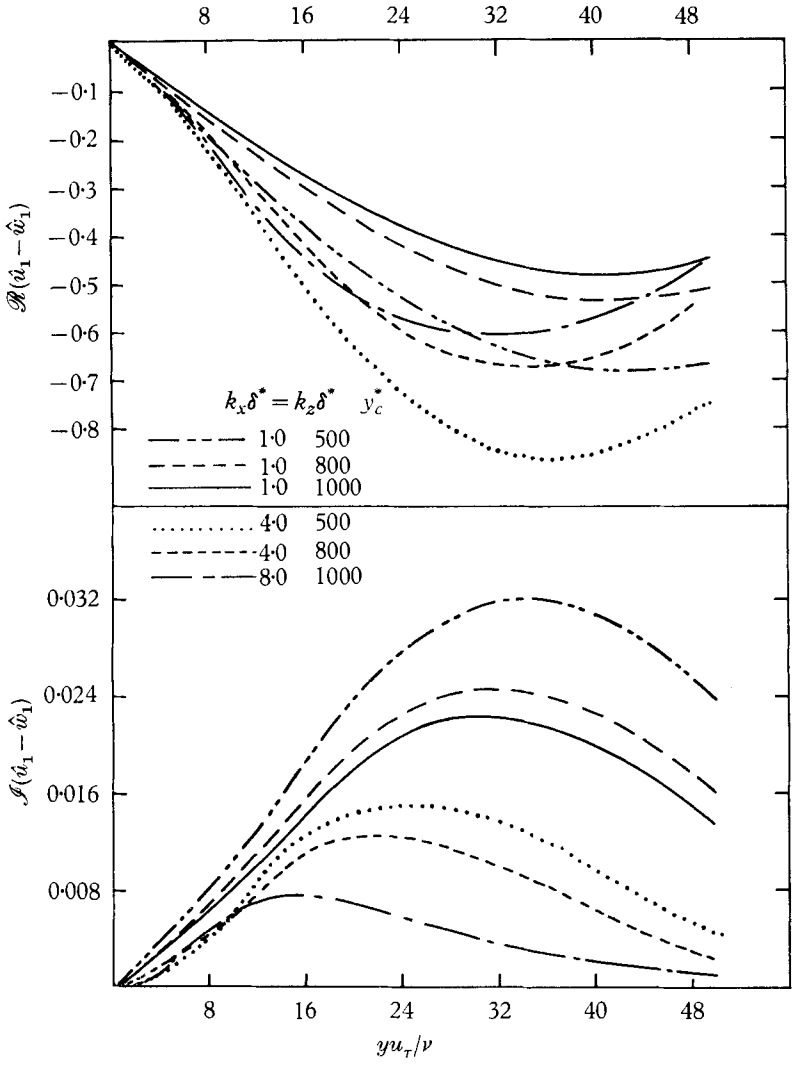

FIGURE 6. The asymptotic shape of $\hat{u}$ for values of k_z/k_x.

which yields reasonable values for $\hat{u}$. The results are shown in table 4. According to this table, C_R decreases systematically as k_x increases from $k_x = 0{\cdot}10$ to $k_x = 10{\cdot}0$. In general, C_R also decreases somewhat at fixed values of $k_x\delta^*$ as y_c^* is increased. Equations (12a, b) show that if θ is large enough, the phase angle between $\hat{u}$ and $\hat{v}$ and therefore the value of C_R remain approximately the same. The range of values of C_R and the tendency for this coefficient to decrease with

increasing longitudinal wave number are in satisfactory agreement with the experimental results of Klebanoff.

It has been seen that the amplitude of $\hat{u}$, $\hat{w}$ and $\hat{v}$ has a measure of arbitrariness since it depends on θ. This is also true of the ratio $\hat{w}/\hat{u}$. However the ratio $\hat{v}/\hat{u}$ varies little with θ for large values of θ. According to table 4 this ratio is generally

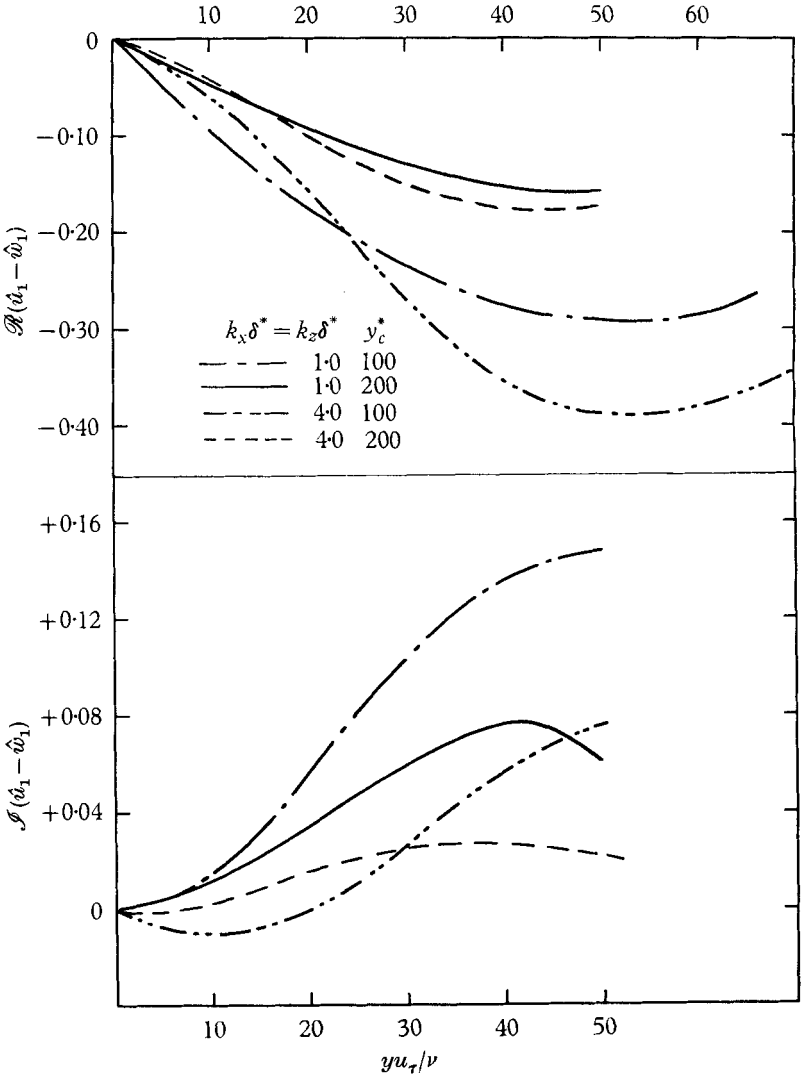

FIGURE 7. The asymptotic shape of $\hat{u}$ for large values of k_z/k_x.

quite small. It varies from about 1 % for $k_x = 0{\cdot}1$ to about 36 % for $k_x = 4{\cdot}0$ ($y_c^* = 500$). According to table 2, while the latter figure is reasonable, the former is not and for the bulk of the solutions, the ratio $\hat{v}/\hat{u}$ must be considered too small. There may be some doubt about the experimental distribution of v' for $y^* < 30$ and *a fortiori*, about the longitudinal spectrum of this quantity in that region (i.e. Klebanoff measured v' only for $y^* > 50$ and a v' spectrum only for $y^* > 150$).

But there is no doubt about the experimental distribution of $\langle uv \rangle$ and little doubt about that of u' so that the smallest possible values of v' for $y^* < 50$ are known to be at least half those shown on figure 2. All the solutions indicate that as y^* increases, the ratios of $\hat{v}/\hat{u}$ and $\hat{w}/\hat{u}$ increase and equations (14) imply that a typical wave-number for component $\hat{w}$ is characterized by a smaller angle θ

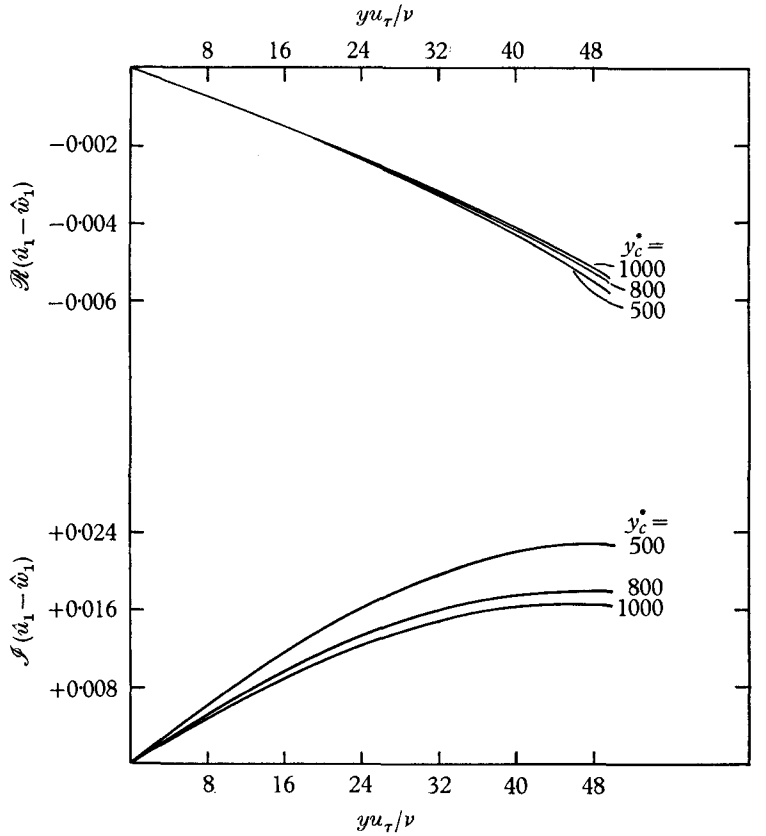

FIGURE 8. The asymptotic shape of $\hat{u}$ for large values of $k_z/k_x . k_x\delta^* = 0{\cdot}1$.

than a typical wave-number for component $\hat{u}$ and $\hat{v}$. Both of these results are in accordance with experimental evidence. Representative solutions indicate that the phase of $\tilde{v}$ lags that of $\tilde{p}$ very nearly by $\frac{1}{2}\pi$. Thus according to the linear model, the expression $\partial/\partial y \langle pv \rangle$, a transport term in the equation for turbulent kinetic energy, is very small. The experimental evidence is inconclusive on this point. The measurements of $\langle pv \rangle$ and $\langle pu \rangle$ covariances by Willmarth & Wooldridge (1963) and by Bull *et al.* (1963) were made for larger values of y^* then those considered in the analysis while measurements by Kawamura (1960) made in a wind tunnel suffering from a high noise level at an artificially low Reynolds number disagree with those of Bull *et al.* and Willmarth & Wooldridge in a number of important respects. At $y^* = 180$, Willmarth & Wooldridge found the phase angle between $\tilde{p}$ and $\tilde{v}$ to be as described above, while $\tilde{u}$ led $\tilde{p}$ by an angle slightly exceeding $\frac{1}{2}\pi$. We note that measurements of $\langle pu \rangle$ in ordinary wind tunnels at

small values of y^* are not especially difficult and it is hoped that such measurements will be published in the future.

In a paper which reached us after this work was completed, Sternberg (1965) examines the inner wall layer by using equations equivalent to (6). His calculations consist of a machine integration of these equations. Sternberg's discussion of the outer boundary conditions he used for this integration is unclear to us. These conditions may be different from ours. Not enough details are given to

	y^*	$\hat{u}'$	$\hat{w}'$	$\hat{v}'$	c_R
$k_x\delta^* = 0{\cdot}1$	10	0·32	0·26	0·00078	+0·65
$y_c^* = 1000$	20	0·51	0·51	0·0031	+0·82
$k_z/k_x = 10$	30	0·69	0·82	0·0067	+0·84
	40	0·78	0·90	0·011	+0·82
	50	0·77	0·99	0·017	+0·81
$k_x\delta^* = 1{\cdot}0$	10	0·34	0·375	0·0015	+0·20
$y_c^* = 100$	20	0·70	0·750	0·009	+0·382
$k_z/k_x = 3{\cdot}0$	30	0·97	1·05	0·020	+0·540
	40	1·10	1·36	0·036	+0·692
	50	1·13	1·70	0·060	+0·725
$k_x\delta^* = 1{\cdot}0$	10	0·277	0·31	0·0055	+0·11
$y_c^* = 500$	20	0·568	0·53	0·0134	+0·33
$k_z/k_x = 5{\cdot}0$	30	0·736	0·70	0·030	+0·40
	40	0·814	0·83	0·048	+0·38
	50	0·750	0·92	0·060	+0·30
$k_x\delta^* = 4{\cdot}0$	10	0·31	0·36	0·022	−0·15
$y_c^* = 500$	20	0·73	0·56	0·067	+0·115
$k_z/k_x = 5{\cdot}0$	30	0·95	0·71	0·13	+0·140
	40	0·93	0·85	0·21	+0·080
	50	0·79	0·93	0·29	+0·065

TABLE 4. The amplitudes of $\hat{u}$, $\hat{v}$, $\hat{w}$ and the Reynolds stress coefficients for large values of θ.

compare the two computations quantitatively. Sternberg verified numerically that certain features of the solutions did not depend critically upon the outer boundary conditions and these features agree with the corresponding results discussed above. For instance, the phase relationship between $\tilde{p}$ and $\tilde{u}$, its dependence on θ and the dependence of the ratio $|\tilde{w}|/|\tilde{u}|$ upon θ are qualitatively very similar in our and Sternberg's work. The same is true of the dependence on θ, of the ratio of the pressure amplitude to that of the downstream component $\tilde{u}$.

13. The dynamics of a typical fluctuation according to the linear approximation

As we have seen, according to linear theory, typical turbulence patterns near the wall are greatly elongated in the streamwise direction because the effective impedance of the layer near the wall is not isotropic (cf. (13)), the ratio of the response $|\tilde{u}|$ or $|\tilde{v}|$ to the forcing function $k\tilde{p}$ increasing asymptotically as $\tan\theta$ (θ is the angle between the direction of the force and the streamwise direction). It is possible to account simply for the main features of the dynamics of such

elongated eddies, including the result that a peak is reached for the amplitude of $\tilde{u}$ for small values of y^*.

For high values of θ, $\partial\tilde{p}/\partial x \ll \partial\tilde{p}/\partial z$ and $\partial\hat{u}/\partial x \ll \partial\hat{w}/\partial z$ so that one may write the x and z momentum and continuity equations as

$$\frac{d^2\tilde{u}}{dy^2} - \frac{i}{\nu}(\omega + k_x U)\tilde{u} \cong \frac{1}{\nu}\frac{dU}{dy}\tilde{v},$$

$$\frac{d^2\tilde{w}}{dy^2} - \frac{i}{\nu}(\omega + k_x U)\tilde{w} = \frac{ik_z}{\mu}\tilde{p},$$

$$ik_z\tilde{w} + \frac{d\tilde{v}}{dy} \cong 0.$$

The asymptotic form (13) embodies the same approximation. These equations imply that the spanwise pressure gradient is the only forcing function of importance. Such a gradient causes a spanwise velocity fluctuation which in turn, according to the continuity equation, causes a normal velocity $\tilde{v}$ proportional to $k_x\tilde{w}$, i.e. to k_z^2. Now $\tilde{v}$ which is multiplied by the mean shear dU/dy in the x-momentum equation then acts as the main forcing function for $\tilde{u}$ fluctuations. Since $\tilde{u}$ vanishes at $y^* = 0$ and since the exponentially increasing homogeneous solution of $\tilde{u}$ is rejected, $\tilde{u}$ would be identically zero according to the approximation, were it not for this forcing term. On the other hand, the mean shear is a very rapidly decreasing function of y^* so that the product $\hat{v}\,\partial U/dy$ is a function which is zero at the origin, rises to some amplitude as $\hat{v}$ increases and then decays again. The solution for $\hat{u}$ then decays also with y^* at a rate which depends on the viscous length which is characteristic of the parameters β, u_c and k_x. Thus according to the linear equations $\hat{u}$ is principally due, not to the pressure gradient $\partial\tilde{p}/\partial x$ but to the displacement of the mean profile by the normal component $\hat{v}$ which is generated by the spanwise component of the pressure. The equation for $\tilde{u}$ is thus related to the model used by Prandtl (1925) in connexion with his mixing length theory to explain the presence of Reynolds stresses. Also, Kistler (1962) had suggested not only that u might not be too closely related to $\partial p/\partial x$ but also that the experimentally observed maximum of u' near the wall might be related to the lateral displacement of the highly sheared mean flow.

14. Summary of the results

The linear equations provide a model of turbulent velocity fluctuations near the wall which in many ways is strongly suggestive of the observed features of these fluctuations. In particular they provide a simple reason (cf. (13) and § 13) why the longitudinal fluctuations experience a peak in amplitude close to the wall, why the turbulent structure is strongly elongated in the direction of the mean flow, why the structure of u and v is more elongated than that of w. They yield solutions which assign plausible phase relationships between $\hat{u}$ and $\hat{v}$ (cf. table 4) and thus allow the fluctuations to extract energy from the mean stream. They describe at least qualitatively the close relationship between the strongly curved mean velocity profile near the wall and the turbulence; this strong curvature is both the cause of Reynolds stresses (by allowing a rapid growth of the part of u

which is in phase with v) and the result of these stresses. Many qualitative features of the flow are echoed in the solutions. For instance the known fact that $\tilde{u}$ and $\tilde{v}$ become more nearly orthogonal in time as k_x increases and which has been ascribed to the tendency of small eddies toward isotropy (a non-linear mechanism) turns out to be also a property of the linear solutions (table 4).

Some of the weaknesses of the solutions presented are: (a) the rise of $\hat{u}$ with y^* is somewhat less rapid than experiments suggest (by a factor of 1·5 to 2); (b) the magnitude of $\hat{v}$ seems too small unless the relevant values of θ are very large: in either case the ratio $\hat{v}/\hat{u}$ is smaller by a factor of 2 to 4 than can be inferred from the data. (a) and (b) taken together imply that the Reynolds stresses generated by the solutions would fall short of those necessary to maintain the mean profile.

The ratios of the amplitudes of the velocity components to that of the pressure become unbounded as $\theta \to \frac{1}{2}\pi$. This does not necessarily mean that the resulting velocity spectra should be unbounded since it is experimentally plausible that $\pi(k_x, k_z) \to 0$ as $k_z \to \infty$ at a rate sufficient to yield finite values for $E(k_x, \infty)$. We note that the analysis which has been presented is based on the assumption that $\partial p/\partial y$ is negligible, which is increasingly inaccurate if k is allowed to become large. Then for every k_x the predictions of the theory may not be extended to arbitrarily large k_z.

15. The role of the non-linear terms

The problem has been formulated in such a way that the solutions for $\tilde{u}$, $\tilde{v}$, $\tilde{w}$ must tend to solutions of the full equations for small enough values of y^*. The relative importance of the non-linear terms as y^* increases may be assessed coarsely by referring both to the experiments and to the linear solutions. Consider first equation (1a) for u. The three omitted terms are very nearly

$$\frac{\partial \tau_{xj}}{\partial x_j} = -u\frac{\partial u}{\partial x} - w\frac{\partial u}{\partial z} - v\frac{\partial u}{\partial y} + \left\langle v\frac{\partial u}{\partial y}\right\rangle.$$

The first term should be small in general since the downstream gradients of u are small, next to spanwise gradients and the magnitude of u and w is comparable. The magnitude of the remaining two terms is probably about the same. One may view these terms as forcing functions along with $\rho^{-1}\partial p/\partial x$ and $v\,\partial U/\partial y$. According to previous discussions we may obtain an estimate of non-linear effects in this equation by comparing these terms to the dominant linear term $v\,\partial U/\partial y$. The solutions for $\hat{u}$ have been found to increase monotonically up to $y^* \cong 30$ so that $\overline{\langle(\partial u/\partial y)^2\rangle}^{\frac{1}{2}}$ is not likely to exceed significantly $d/dy\,\langle u^2\rangle^{\frac{1}{2}}$. From extrapolations of data from Klebanoff and other sources one may estimate that up to $y^* = 30$, $(v\,\partial u/\partial y - \langle v\,\partial u/\partial y\rangle)$ does not exceed 20–30 % of $v\,\partial U/\partial y$. As y^* increases, the ratio of mean shear to turbulent shear $\langle(\partial u/\partial y)^2\rangle^{\frac{1}{2}}$ decreases steadily. It is about unity for $y^* = 80$ and about $\frac{1}{4}$ or less for $y^* = 200$. Thus while neglect of the non-linear terms may be barely tolerable at $y^* = 30$ it seems indefensible for $y^* = 200$. In the spanwise momentum equation, the two non-linear terms $v\,\partial w/\partial y$ and $w\,\partial w/\partial z$ should be compared to the pressure gradient $\rho^{-1}\partial p/\partial z$. In view of the facts (cf. Grant 1958; Klebanoff 1954) that w' is somewhat smaller than u',

that $\partial w'/\partial y$ is noticeably smaller than $\partial u'/\partial y$ near the wall, and that the structure of w is a good deal less elongated than that of u, it is likely that these terms are no more important in the spanwise momentum equation than their counterparts in the streamwise equation up to $y^* = 30$.

For Fourier components such that the value of θ is small, it is almost certain that the non-linear terms cannot be neglected even for very small values of y^*. This would seem to be a consequence of the strong dependence of velocity amplitudes on the ratio k_z/k_x. Non-linear terms enter the transformed equations as convolution integrals of the form

$$\int f(\mathbf{k}', \omega')\, g(\mathbf{k}-\mathbf{k}', \omega-\omega')\, d\mathbf{k}'\, d\omega',$$

where f and g are typical Fourier components of velocities or velocity gradients. For $k_z/k_x \leqslant 1$ the amplitudes of $f(\mathbf{k}, \omega)$ and $g(\mathbf{k}, \omega)$ are small but $\mathbf{k}'$ and $\mathbf{k}-\mathbf{k}'$ may evidently be such that while their inclination angle θ to the k_x axis is close to $\frac{1}{2}\pi$, their sum $\mathbf{k}$ is such that $k_z/k_x \leqslant 1$.

The plausibility of some of the main features of the solutions which have been presented suggests that a similar analysis for a boundary layer along a compliant wall might reveal whether and under what circumstances a compliant wall inhibits or amplifies turbulence.

The authors wish to thank Dr T. Brooke Benjamin for summarizing some general results of the present work (as well as his own) in a survey lecture for the 11th Congress of Applied Mechanics (Munich, 1964), for discussions, and for suggestions regarding the draft of this paper.

REFERENCES

BULL, M. K., WILBY, J. F. & BLACKMAN, D. R. 1963 *Univ. of Southampton AASU Rept.* no. 243, part 1.

COLES, D. 1953 *Jet Propulsion Laboratory Rept.* no. 20–69.

CORCOS, G. M. 1964 *J. Fluid Mech.* **18**, 353.

EINSTEIN, H. A. & LI, H. 1956 *ASCE Proc.* **82**, no. EM 2.

GRANT, H. L. 1958 *J. Fluid Mech.* **4**, 149.

HANRATTY, T. J. 1956 *AICHE J.* **2**, no. 3, 359–362.

KAWAMURA, M. 1960 *J. Science, Hiroshima Univ.* (Series A), **241**, 403.

KISTLER, A. 1962 Mecanique de la Turbulence, Centre National de la Recherche Scientifique, Publication no. 108, 287.

KLEBANOFF, P. W. 1954 *NACA Technical note* no. 3178.

LANDAHL, M. 1965 A wave-guide model for turbulent shear flow. *NASA CR* 317.

LIGHTHILL, M. J. 1963 *Laminar Boundary Layers* (L. Rosenhead, editor). Oxford: Clarendon Press.

LILLEY, G. M. 1963 *AGARD Rept.* no. 454.

PRANDTL, L. 1925 *ZAMM*, **5**, 136.

PRIESTLEY, J. T. 1965 *National Bureau of Standards, Rept.* no. 8942.

SCHLICHTING, H. 1960 *Boundary Layer Theory*. London: Pergamon Press.

STERNBERG, J. 1962 *J. Fluid Mech.* **13**, 241.

STERNBERG, J. 1965 *AGARDOGRAPH* 97.

WILLMARTH, W. W. & WOOLDRIDGE, C. F. 1962 *J. Fluid Mech.* **14**, 187.

WILLMARTH, W. W. & WOOLDRIDGE, C. F. 1963 *AGARD Rept.* no. 456.